Thin–Walled Structures 199 (2024) 111808

Contents lists available at ScienceDirect

Thin-Walled Structures

journal homepage: www.elsevier.com/locate/tws

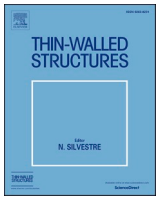

Full length article

Interaction diagrams of thin-walled, open cross section PC beams

Marco Andrea Pisani

Department of Architecture, Built Environment and Construction Engineering, Politecnico di Milano, Piazza Leonardo da Vinci 32, 20133, Milan, Italy

ARTICLE INFO

Keywords:
Torsion
Inelastic warping
Ultimate
Interaction diagrams
Prestressed concrete

ABSTRACT

Thin-walled, open cross section PC (prestressed concrete) beams are widely used in precast structures. Nevertheless, the analytical computation of their load carrying capacity under bending and torsion is still an unsolved problem. This is because of the markedly non-linear behaviour of both steel and concrete and of the asymmetry of the behaviour of concrete in tension and compression. This involves a search for the correct solution from a physical point of view (among those mathematically admissible) based on trial-and-error methods of numerical analysis.

This paper suggests a method to evaluate the interaction diagrams under bending and torsion. According to this method the solving system is made by two equilibrium plus two compatibility equations. Some examples show the outcomes of this approach.

1. Introduction

For over half a century, thin-walled, PC (prestressed concrete) open cross section beams have been widely used in precast structures. Their use is particularly widespread in the construction of roofs for industrial sheds and warehouses, as well as in the construction of floors in shopping centres and multi-storey car parks. Nevertheless, research into the mechanical response of open thin-walled PC members under combined actions of bending, shear and torsion is quite rare. This is because of the extreme complexity of the problem.

It is well established [1–5] that, the torsional behaviour of thin-walled sections is the combination of the torsional behaviour according to St. Venant's theory, and the one related to warping deformation, which implies the distortion of the cross section out of its own plane. The second effect is described by means of a particular internal action, called bimoment (or warping moment), which gives rise to a normal stress distribution that adds to the one coming from bending of the beam and is comparable to it. Moreover, this phenomenon gives rise to a shear stress that adds to those related to both circulatory torque and shear.

When dealing with simply supported, open cross section P.C. beams it is usually possible to partially simplify the problem by ignoring the shear stress related to circulatory torque owing to the small thickness of the members composing the cross section [9], but nevertheless their analysis is extremely complicated, due to the non-linear constitutive laws that have to be adopted for the materials involved.

The tensile strength of concrete is about one tenth of that under compression, and once concrete cracks that crack will last all the structural member lifelong (at least 50 years according to the codes [7]). Moreover, Leonhardt [8] lists twenty possible causes of crack formation prior to the first application of the load. In short, the tensile strength of concrete can't be taken into account and steel reinforcing bars and tendons are placed to supply this weakness. According to the European Codes [7], the constitutive law that have to be adopted to determine the load carrying capacity related to the stress normal to the cross section of these beams are depicted in red in Fig. 1.

The adoption of these non-monotonic constitutive laws inevitably entails an enormous complication of the problem since from a mathematical point of view it may have no solution, a finite number or even an infinite number, depending on the values of the internal actions involved. It is up to us to find the correct solution, i.e. the real (experimental) one.

Moreover, the piecewise curvilinear shape of the constitutive laws adopted implies the knowledge of the strain distribution over the structural element to determine which curvilinear segment of the constitutive law has to be adopted point by point to determine the stress distribution, but this would imply the knowledge of the solution. For example, the cracked zones of the cross section are marked in red in Fig. 12 in the three cases where the strain distribution at the ultimate limit state is depicted.

In short, the determination of the solution is an implicit problem in the terminology of numerical analysis (that is one can't write the solving system if he does not know the solution). This implies the need to adopt a trial-and-error method of numerical analysis, which inevitably brings

E-mail address: marcoandrea.pisani@polimi.it.

https://doi.org/10.1016/j.tws.2024.111808
Received 6 November 2023; Received in revised form 11 March 2024; Accepted 15 March 2024
Available online 19 March 2024

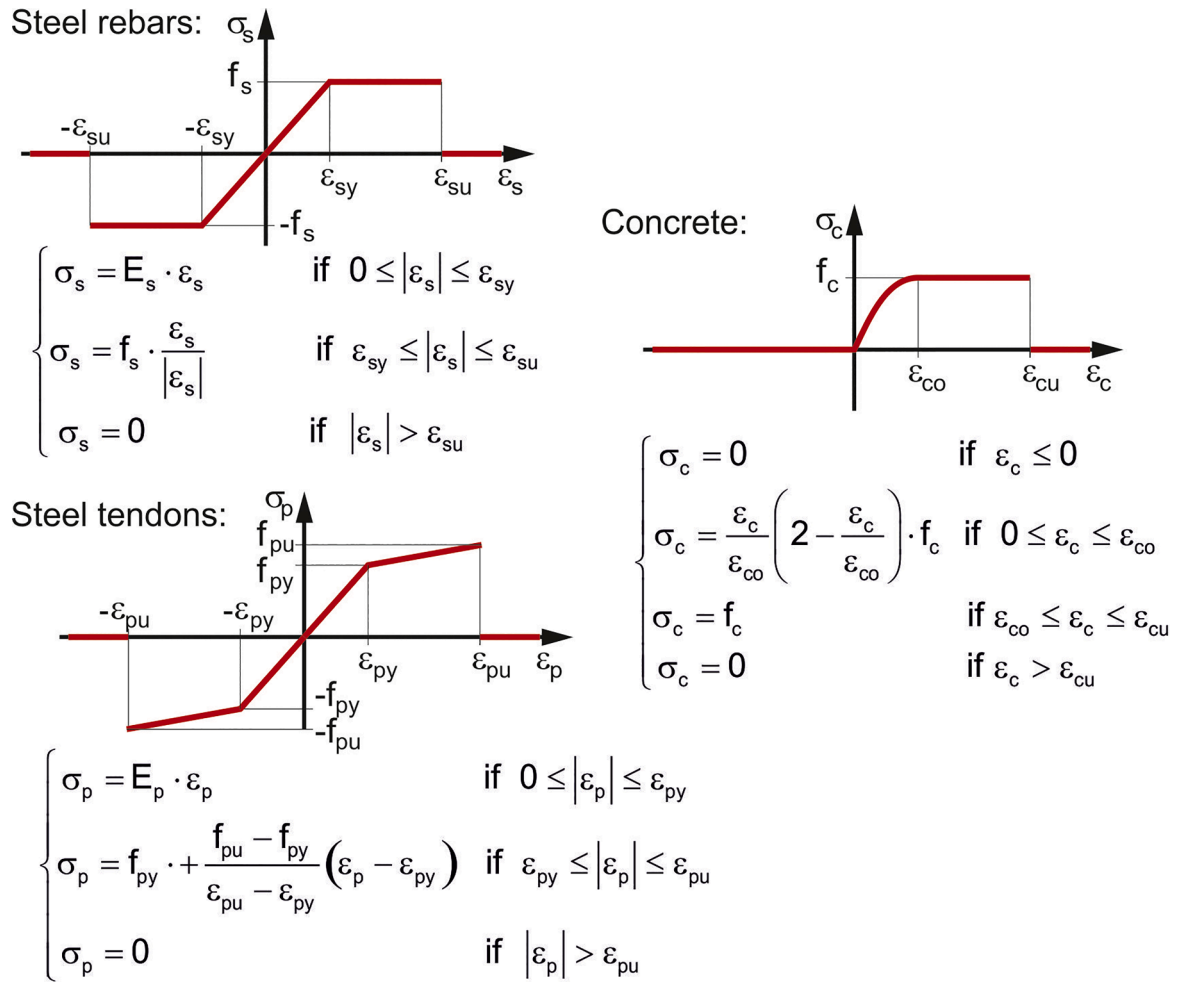

Fig. 1. Constitutive laws for steel and concrete (compression is positive).

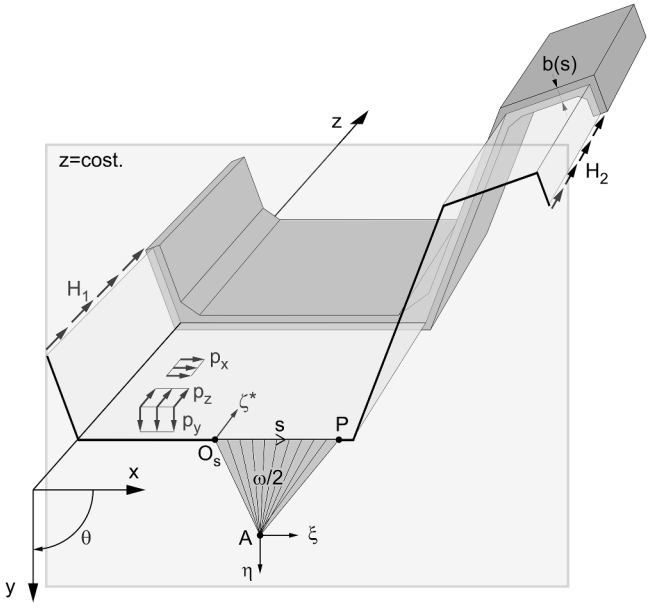

Fig. 2. Section characteristics, sectorial area, and loads.

with it all the problems related to its convergence to the solution sought, i.e. the real (experimental) one. Note that the position of the shear centre changes with the level of damage, that is the level of stress over the cross section. Because of this, the computation of the interaction diagrams of thin-walled, open cross section PC beams will be made according to Vlasov's torsion theory, except for the constitutive laws of the materials and the effect of prestressing. More sophisticated approaches that take into account the shear lag effect [9–11] are not needed. This is because in these simply supported beams the shear influence is small, owing to the high value of the span to cross-section height ratio [12] which is between 12 and 24.

Although complicated, the analysis under long-term service loads (that takes into account the delayed behaviour of concrete, i.e. creep and shrinkage) can still be conducted according to established rules and methods [13–17].

As far as the determination of the load carrying capacity is concerned, to date the most used method in professional practice to determine it consists in carrying out a sufficient number of destructive experimental tests (see for instance [18–24] and [25]. Of course, this practice is justified in the case of mass production, which, moreover, is current practice for this type of precast elements.

Without prejudice to the fact that a non-linear finite element analysis of a heterogeneous beam [26–28] is currently not feasible in common practice, the only viable alternative is to try to extend to these beams the methods and techniques normally adopted for compact cross section and thin-walled closed cross section beams, i.e. carry out separate checks for normal stress around midspan and shear stress at the supports at ultimate. Both these stress distributions are modified by the presence of the warping torsion.

The topic of determining the strength for shear stress is extremely complex and not yet solved. Moreover, few scientific publications deal

with this topic [29-30,25].

In the case of double tee or U-shaped sections, in common practice the problem is normally simplified by assigning to the two vertical members the task of collecting the twisting moment applied through their bending in opposite directions. These bendings give rise to V_T shear actions in opposite directions, that is to a resistant torque $V_T \cdot d$ where d is the (horizontal) distance between the axes of the two vertical members. Therefore, once the twisting moment has been assigned and d is known, the shear V_T is immediately obtained. By adding V_T to the shear action due to the vertical bending of the beam, it is possible to carry out the shear verification of each vertical element, taken individually (i.e. as an individual structural element).

Naturally this approach is not applicable to sections of a more complex and asymmetrical shape, such as that of Fig. 2. However, it should be noted that the shear stress due to warping is constant over the thickness of each member of the cross section and therefore is comparable to an increase in the stress present in the same member due to the shear action. Therefore, if the shear action resulting from the bending and torsion effects could be defined for each member of the cross section, a truss model could be subsequently adopted, i.e. one could think of applying the same rules used for the shear verification of a rectangular section coinciding with the member under examination. It follows that in complex cases the approach often adopted is to calculate the overall shear stress with Vlasov's theory (linear elasticity) and then assume their integral made over the member's area as shear action acting on that member. The weakness of this approach lies in the fact that Vlasov's elastic theory should be revised due to the cracking of concrete.

It remains to determine the behaviour of the beam due to normal stress.

Regarding the verification under assigned internal actions, few works are available in the literature [29,31] supported by the experiments test reported in [30], and to the author's knowledge nothing is available on the subject of calculating interaction diagrams. This is the topic that will be discussed in this paper, whose aim is to evaluate the load carrying capacity of the cross section related to normal stress through the determination of the interaction diagrams.

It should be noted that even if experimental qualification tests are carried out, the numerical analyses mentioned above are essential in the design phase, in order to obtain prototypes that can give satisfactory experimental results.

2. Flexural-torsional behaviour of the heterogeneous cross section, problem setting

The four hypotheses adopted in Vlasov's theory are:

- the thin-walled open cross section is non-deformable in its plane (i.e. the cross section shape does not change);
- the shear strain of the middle surface can be ignored;
- the normal stress in the direction of the generator of the middle surface and the tangential stresses in the direction of the tangent to the profile line are the only stresses considered;
- the normal and tangential stresses are constant over the thickness of a member.

The first two hypotheses are of geometric type, and as such they apply regardless of the shape of the constitutive law of the materials. Consequently, the equations that describe the axial strain $\varepsilon_c(z,s)$ of concrete at a generic point P, whose position on the profile line placed at z = const. (z being an arbitrary axis parallel to the beam axis, see Fig. 2; const. = constant value, i.e. the cross section under investigation) is set by means of the curvilinear coordinate s (taken with an arbitrary origin O_s), are [3]:

$$\begin{aligned}\zeta(z) &= \zeta^*(z) + \xi'(z)\cdot x|_{s=0} + \eta'(z)\cdot y|_{s=0}\\ \varepsilon_c(z,s) &= \zeta'(z) - \xi''(z)\cdot x(s) - \eta''(z)\cdot y(s) - \theta''(z)\cdot\omega(s)\end{aligned} \tag{1}$$

where:

- all the derivatives are made with respect to z;
- x and y are two arbitrary Cartesian axes orthogonal to z axis;
- ζ^* is the displacement of point O_s in the direction of the z axis;
- θ is the rotation around the z axis of the plan z = const.;
- ξ and η, respectively, are the displacements in the x and y direction of a generic point A placed over the z = const. plan;
- ω is the sectorial area measured between point A, the sectorial origin O_s, and point P (see Fig. 2), i.e., the coordinate that depends on the shape of the mean profile of the thin-walled cross section.

The last two hypotheses refer to the stress distribution, that is to say they do not take into account the constitutive laws adopted for the materials. Therefore, the equilibrium equations built with them do not change with respect to the linear elastic case, that is [3]:

$$\begin{aligned}&\frac{\partial N(z)}{\partial z} = -\int_L p_z(z,s)ds - \sum_r H_r(z)\\ &\frac{\partial^2 M_x(z)}{\partial z^2} = -\int_L \frac{\partial p_z(z,s)}{\partial z}\cdot x(z)ds - \int_L p_x(z,s)ds - \sum_r H_r(z)\cdot x(s_i)\\ &\frac{\partial^2 M_y(z)}{\partial z^2} = -\int_L \frac{\partial p_z(z,s)}{\partial z}\cdot y(z)ds - \int_L p_y(z,s)ds - \sum_r H_r(z)\cdot y(s_i)\\ &\frac{\partial^2 M_\omega(z)}{\partial z^2} + \frac{\partial T_{SV}(z)}{\partial z} = -\int_L \frac{\partial p_z(z,s)}{\partial z}\cdot\omega(z)ds - \sum_r H_r(z)\cdot\omega(s_i) +\\ &-\int_L \left[p_y(z,s)\cdot(x(s)-x_A) - p_x(z,s)\cdot(y(s)-y_A)\right]ds\end{aligned} \tag{2}$$

$$\begin{aligned}N(z) &= \int_L \sigma_c(z,s)\cdot b(s)ds + \sum_{m=1}^{n_s}\sigma_{s_m}(z)\cdot A_{s_m} + \sum_{n=1}^{n_p}\sigma_{p_n}(z)\cdot A_{p_n}\\ M_x(z) &= \int_L \sigma_c(z,s)\cdot b(s)\cdot x(s)ds + \sum_{m=1}^{n_s}\sigma_{s_m}(z)\cdot x_{s_m}\cdot A_{s_m} + \sum_{n=1}^{n_p}\sigma_{p_n}(z)\cdot x_{p_n}\cdot A_{p_n}\\ M_y(z) &= \int_L \sigma_c(z,s)\cdot b(s)\cdot y(s)ds + \sum_{m=1}^{n_s}\sigma_{s_m}(z)\cdot y_{s_m}\cdot A_{s_m} + \sum_{n=1}^{n_p}\sigma_{p_n}(z)\cdot y_{p_n}\cdot A_{p_n}\\ M_\omega(z) &= \int_L \sigma_c(z,s)\cdot b(s)\cdot\omega(s)ds + \sum_{m=1}^{n_s}\sigma_{s_m}(z)\cdot\omega_{s_m}\cdot A_{s_m} + \sum_{n=1}^{n_p}\sigma_{p_n}(z)\cdot\omega_{p_n}\cdot A_{p_n}\end{aligned} \tag{3}$$

where:

- the heterogeneity of the cross section is taken into account by considering the concrete section (index c), n_s steel rebars (index s) and n_p prestressing steel tendons (index p)
- $p_x(z,s)$, $p_y(z,s)$ and $p_z(z,s)$ are the external loads per unit surface acting on the beam;
- $M_\omega(z)$ is the bimoment [warping torsion $T_\omega(z) = \partial M_\omega(z)/\partial z$]
- T_{SV} is the Saint Venant torsional moment that in the following will be discarded. Indeed, in the usual commercial thin-walled open cross section beams the parameter $\chi = \sqrt{\frac{GK\ell^2}{EI_{\omega\omega}}}$ ($EI_{\omega\omega}$ is the warping rigidity, GK the Sant Venant torsion rigidity and ℓ the span of the beam) is lower than 2 and therefore warping torsion is dominant [6];
- $H_r(z)$ represents the loads per unit length acting on the lateral edges of the beam;

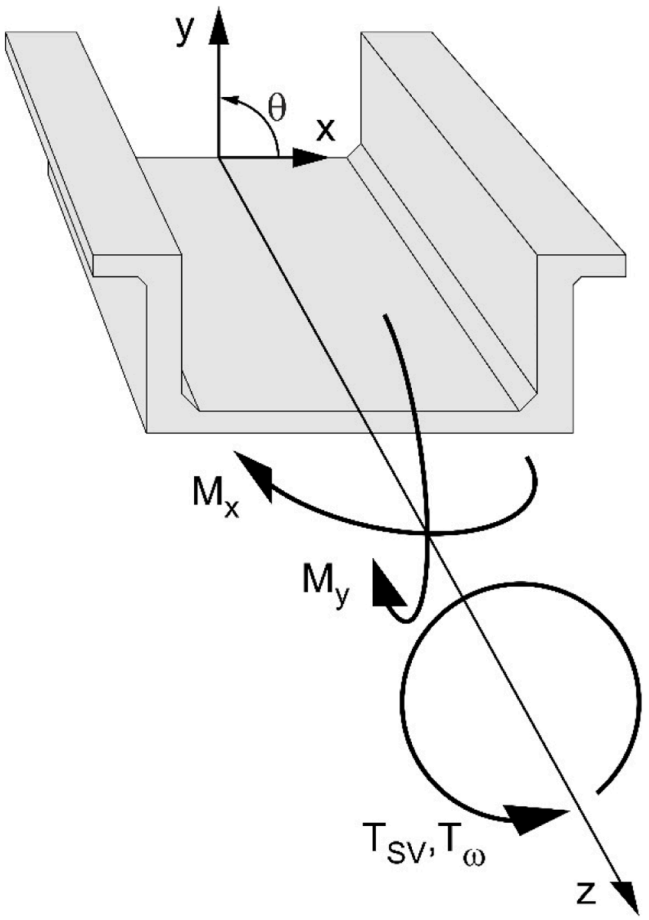

Fig. 3. Positive internal actions in the beam.

- A_{s_m} and A_{p_n} are the areas of the mth rebar and of the nth tendon, whose coordinates are respectively $(x_{s_m}, y_{s_m}, \omega_{s_m})$ and $(x_{p_n}, y_{p_n}, \omega_{p_n})$:
- b(s) is the thickness of the cross section;
- stresses and strains are assumed to be positive if in compression, and the positive internal actions in the beam are drawn in Fig. 3.

The hypothesis of perfect bond between reinforcement and concrete is written as follows:

$$\begin{aligned} \varepsilon_{s_m}(z) &= \varepsilon_c(z,s)|_{s=s_{sm}} \\ \varepsilon_{p_n}(z) &= \varepsilon_c(z,s)|_{s=s_{p_n}} + \bar{\bar{\varepsilon}}_{p_n}(z) \end{aligned} \tag{4}$$

where:

- s_{s_m} and s_{p_n} are the curvilinear coordinates of the mth rebar and of the nth tendon in section z;
- $\bar{\bar{\varepsilon}}_{p_n}(z)$ is the term generally named pre-strain. This term represents prestressing and takes also into account its time evolution due to the delayed behaviour of concrete (creep and shrinkage). Note that this approach to prestressing at ultimate is mathematically exact, as demonstrated in [32].

The non-linear constitutive law of a material can be written as a linear function of the strain and of the secant modulus (superscript *) passing through the origin and through the point corresponding to the current stress level in the stress-strain diagram of this material, i.e.:

$$\begin{aligned} \sigma_c(z,s) &= E_c^*(\varepsilon_c(z,s))\cdot\varepsilon_c(z,s) \\ \sigma_{s_m}(z) &= E_s^*(\varepsilon_{s_m}(z))\cdot\varepsilon_{s_m}(z) \\ \sigma_{p_n}(z) &= E_p^*(\varepsilon_{p_n}(z))\cdot\varepsilon_{p_n}(z) \end{aligned} \tag{5}$$

So doing, the non-linearity is taken into account by means of the secant moduli, that replace in the computation the constitutive laws.

When setting z, that is when assigning both the cross section under investigation and the internal actions acting on it, Eqs. (1), (3), (4) and (5) are no more functions of the independent variable z. Replacing Eqs. (1), (4) and (5) into Eq. (3) one then gets:

$$\mathbf{W}\cdot\boldsymbol{\psi} = \mathbf{M} - \mathbf{F} \tag{6}$$

where $\boldsymbol{\psi}$ is the vector of the unknowns (the terms depending on z in the second of Eqs. (1)), $\mathbf{M}$ is the vector of the internal actions acting on section z, $\mathbf{F}$ is the vector that accounts for the pre-strain. The generic term of matrix $\mathbf{W}$ and of vector $\mathbf{F}$ are written as follows:

$$\begin{aligned} W_{ik} &= \int_L E_c^*(\varepsilon_c(s))\cdot\rho_i(s)\cdot\rho_k(s)\cdot b(s)ds + \\ &+ \sum_{m=1}^{n_s} E_s^*(\varepsilon_c(s_{s_m}))\cdot\rho_i(s_{s_m})\cdot\rho_k(s_{s_m})\cdot A_{s_m} + \sum_{n=1}^{n_p} E_p^*\left(\varepsilon_c\left(s_{p_n}\right) + \bar{\bar{\varepsilon}}_{p_n}\right)\cdot\rho_i\left(s_{p_n}\right)\cdot\rho_k\left(s_{p_n}\right)\cdot A_{p_n} \\ F_i &= \sum_{n=1}^{n_p} E_p^*\left(\varepsilon_c\left(s_{p_n}\right) + \bar{\bar{\varepsilon}}_{p_n}\right)\cdot\rho_i\left(s_{p_n}\right)\cdot A_{p_n}\cdot\bar{\bar{\varepsilon}}_{p_n} \end{aligned} \tag{7}$$

where $\rho_j(s)$ stands for the jth coordinate, i.e. the jth term of vector $|\,1 \quad x(s) \quad y(s) \quad \omega(s)\,|$.

3. How to determine the interaction diagrams

Eq. (6) is a system of four non-linear equations. Since the value of the secant modulus (i.e. the non-linear terms inside Eqs. (6)) to be assigned point by point depends on the local deformation and therefore ultimately on the solution of the problem, the determination of the latter can be obtained only through numerical analysis methods.

In general, the search for the interaction diagram would give rise to a surface in a four-dimensional space, in which the independent variables are the terms of the vector $\boldsymbol{\psi}$. However, when dealing with beams, the axial force is normally zero, so the interaction diagram is reduced to three-dimensional and can be described through a series of two-dimensional domains that represent its level lines (see Fig. 4).

If one wants to determine the domain for assigned values of two internal actions, for example of N and M_x, one can use the corresponding equations of system (6), in which the terms of the vector $\mathbf{M}$ are now known:

$$\sum_{k=1}^{4} W_{ik}\cdot\psi_k = M_i - F_i (\mathrm{i} = 1,2) \tag{8}$$

which will then be associated with the conditions that require the ultimate deformation of the materials not to be exceeded:

$$\begin{aligned} &\varepsilon_c(s)|_{s=s_j} \le \varepsilon_{cu} \\ &|\varepsilon_{s_m}| \le \varepsilon_{su} \\ &|\varepsilon_{p_n}| \le \varepsilon_{pu} \end{aligned} \tag{9}$$

where s_j is the curvilinear coordinate of one of the vertexes that describe the polygonal shape of the concrete cross section.

The calculation procedure consists in first searching for all the points of the two-dimensional domain for which two of (9) are satisfied with the equality sign. This can be done by combining each of (9) with the others. For each combination, a system composed of the two non-linear,

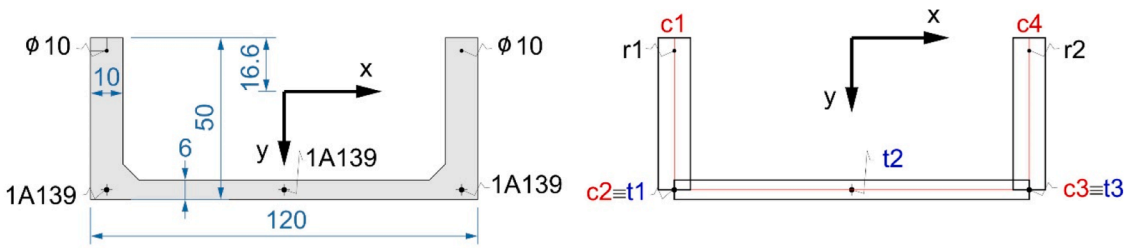

[dimensions are in cm, A139 stands for a 0.6" seven wire stand area=139 mm^2]

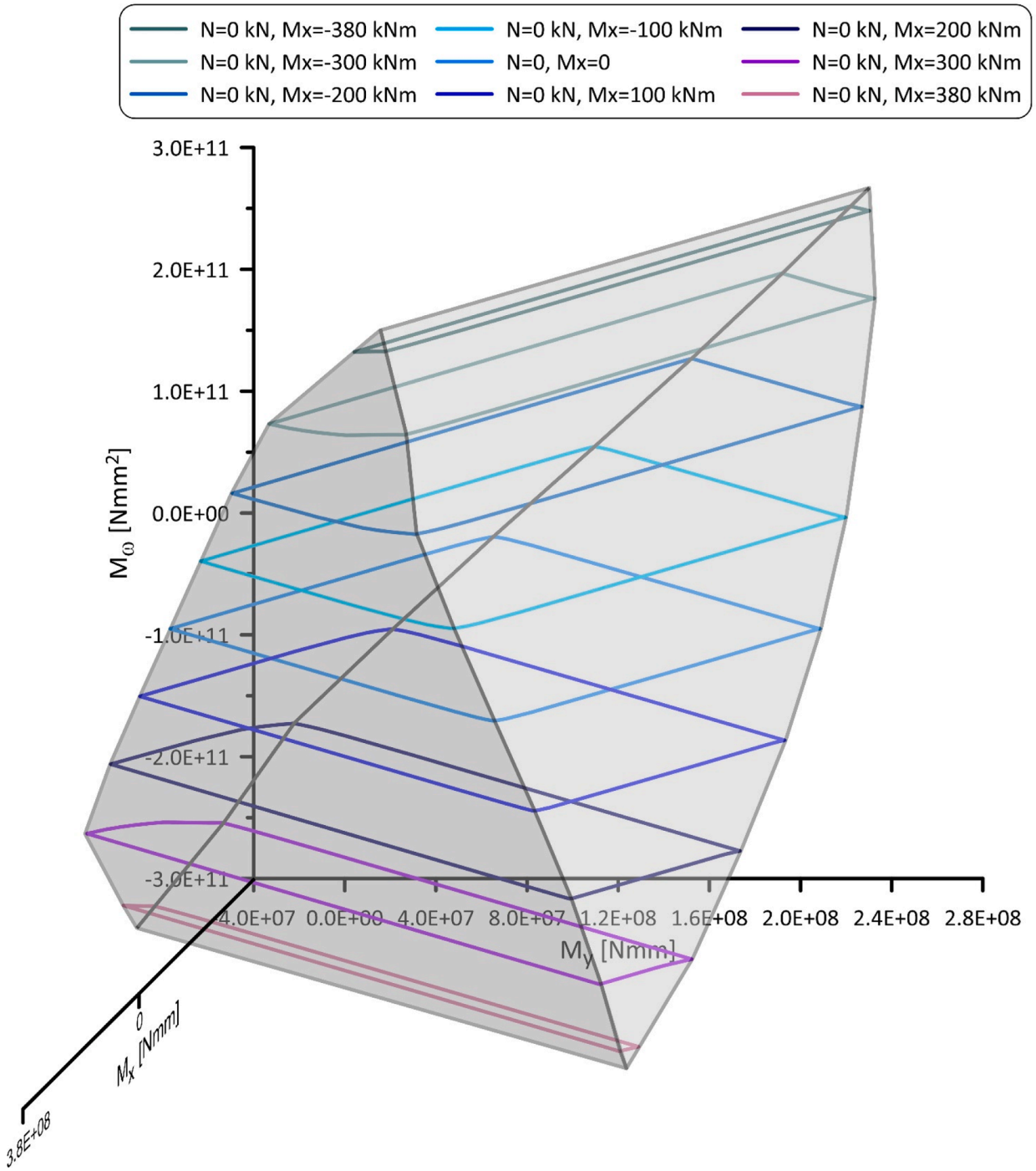

Fig. 4. Three-dimensional interaction diagrams.

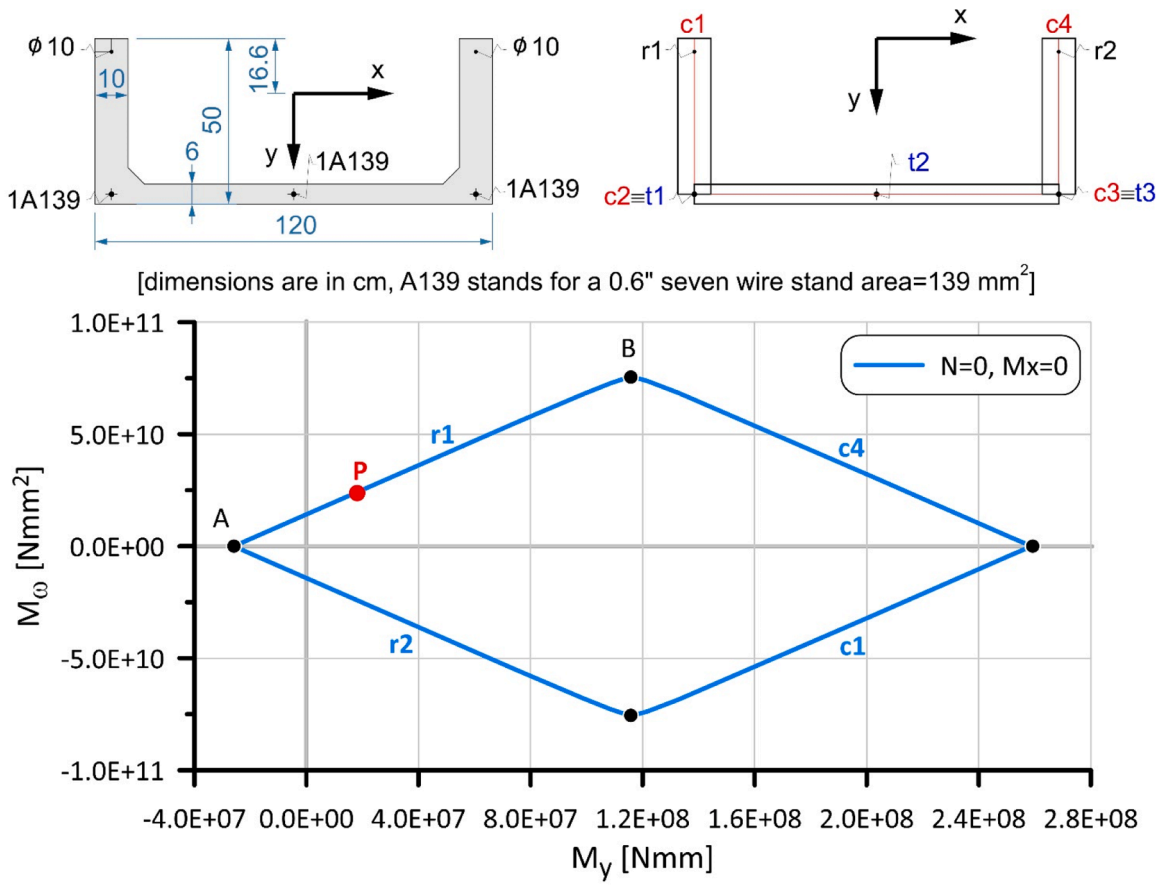

Fig. 5. Two-dimensional interaction diagram.

equilibrium equations (8) and two linear, compatibility equations (9), assumed with the equality sign is thus obtained.

If n_c is the number of nodes that describe the piecewise polygonal shape of the concrete cross section, n_s the number of rebars and n_p that of the tendons, the number N of possible combinations is:

$$N = \frac{(n_c + n_s + n_p - 1)(n_c + n_s + n_p)}{2} \tag{10}$$

this expression shows that as the complexity of the section increases, the number of necessary operations increases quadratically.

The points in which at least two of Eqs. (9) are satisfied with the equality sign represent the common boundary for two different collapse mechanisms of the two-dimensional domain, see Fig. 5. Each of these collapse mechanisms involves the satisfaction of only one of Eqs. (9) with the equality sign, which will also be shared by the two points now calculated that represent its extremes (i.e. pointa A and B in Fig. 5). Without prejudice to this relation as well as Eqs. (8), the residual equation necessary to determine by points the zone of the boundary of the domain corresponding to an assigned failure mechanism, can be obtained by assuming for one of the unknowns of the $\boldsymbol{\psi}$ vector a value between those assumed in the aforementioned extremes, that is, for instance:

$$\omega = \omega_A + (\omega_B - \omega_A)\cdot\gamma 0 \le \gamma \le 1 \tag{11}$$

Whether one is calculating the border point between two failure mechanisms, or one is computing a point of the interaction diagram between the previous ones, the solving system is composed of the two non-linear, equilibrium equations and two linear, compatibility equations. This system has to be solved iteratively. A trial and error method was adopted [33–35]. However, it should be noted that this system is ill-conditioned and can even be singular (i.e. it can be rank-deficient). In fact, if the two equilibrium equations are linearly independent of each other, just as the compatibility equations are, it does not mean that the compatibility equations are linearly independent of the equilibrium ones. May be that due to an unfortunate choice of the reference system one column of the coefficient matrix is a linear combination of the others. In the numerical tests carried out, a very low probability of such an event was found when the centroid of the geometric section is chosen as the origin. Moreover, the adoption of Cramer's rule allows one to reduce the problems associated with ill-conditioning and to detect rank-deficiencies.

By using a trial and error method, during the iterative process there may be trials in which at some point of the cross section the ultimate strain is exceeded. In order to achieve iterative convergence, it is necessary to obtain a result (a numerical value) even in these cases. An expedient to get this numerical value and hence to favour the convergence of the iterative process consists in adding to the constitutive laws of the materials a linear elastic segment after ultimate. The choice of an elastic segment is dictated both by its simplicity, and by the observation that if the constitutive law of materials is a monotonically increasing function, the adoption of the elastic segments after ultimate will keep its monotonic behaviour.

The integrals appearing in the first of Eqs. (7) are solved with easy-to-

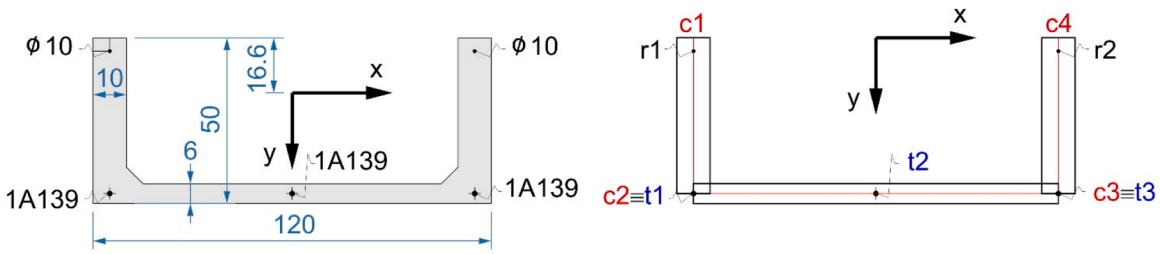

[dimensions are in cm, A139 stands for a 0.6" seven wire stand area=139 mm^2]

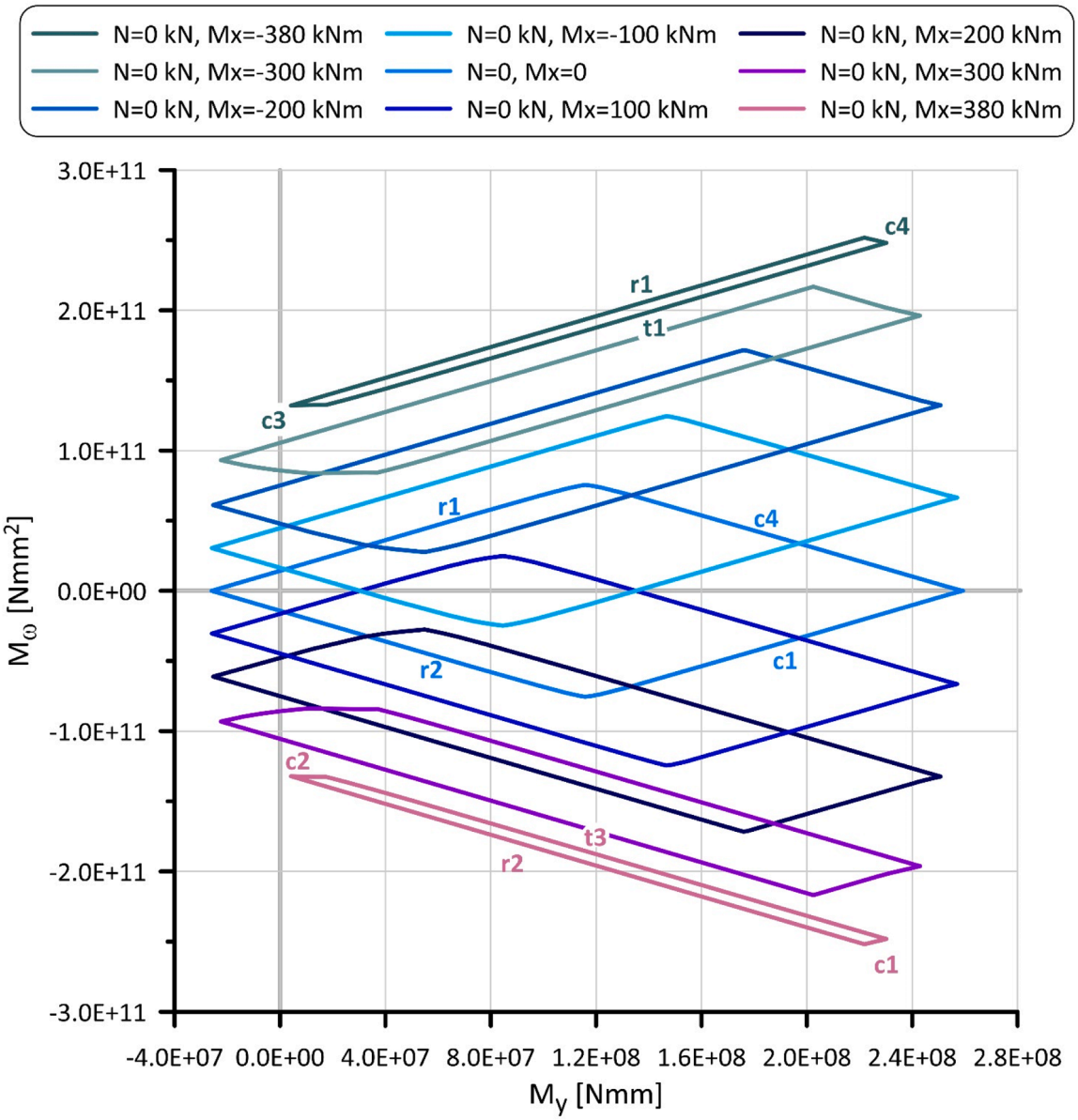

Fig. 6. Complete set of interaction diagrams.

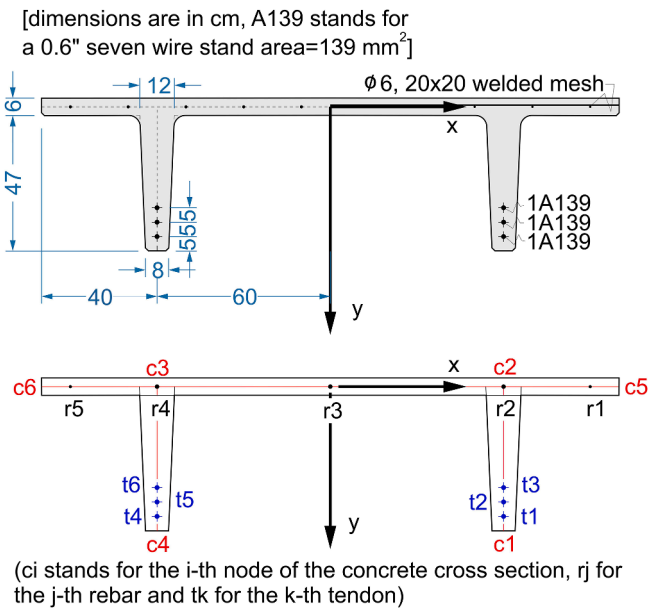

Fig. 7. Geometry of the double tee beam.

determine analytical expressions. This choice allows to reduce the margin of approximation of the calculation and therefore favours the convergence of the iterative process.

Once the system has been solved, it is verified that the remaining Eqs. (9) are satisfied. If this is not true, the calculated solution represents a point outside the interaction diagram and will therefore be discarded, otherwise the two unknown internal actions can be calculated using the two equilibrium equations (8) which have not yet been used.

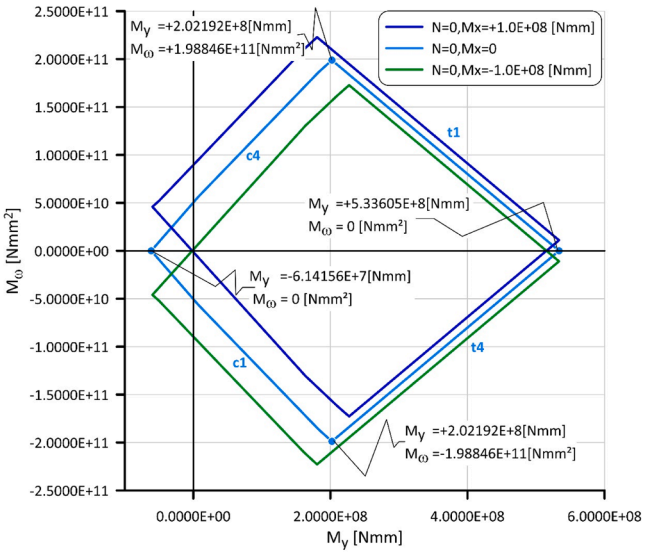

Fig. 9. Interaction diagrams of the double tee beam of practical interest.

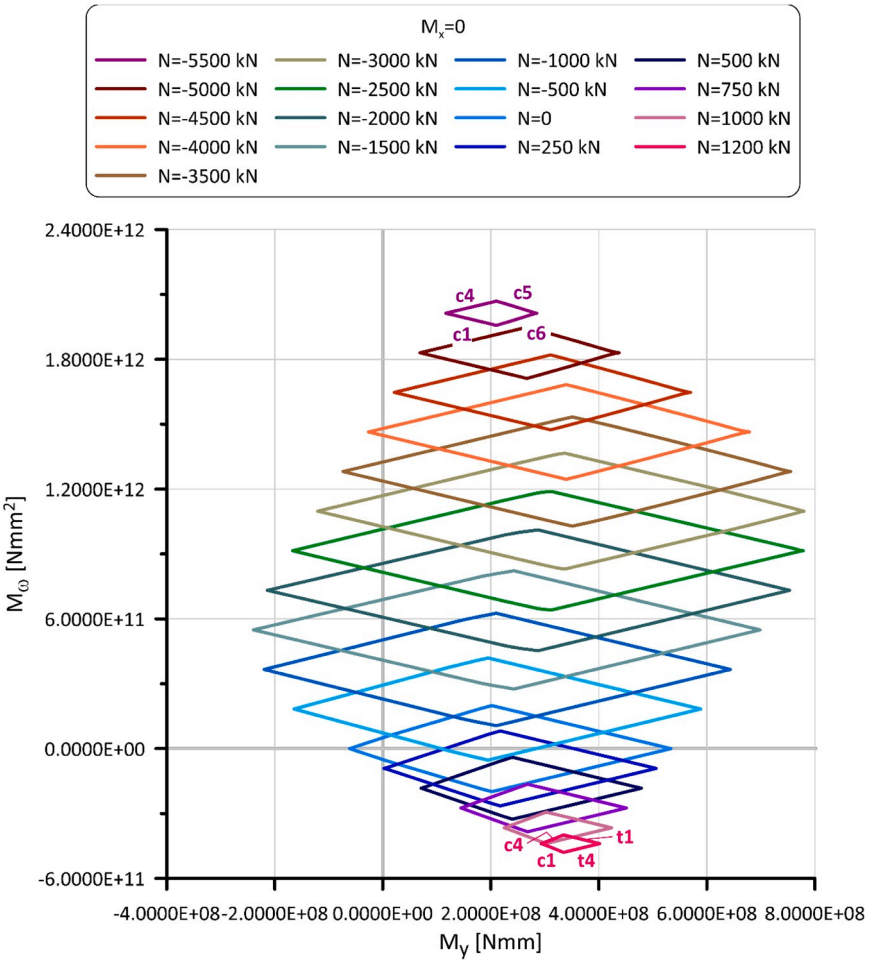

Fig. 8. Interaction diagrams of the double tee beam when M_x=0.

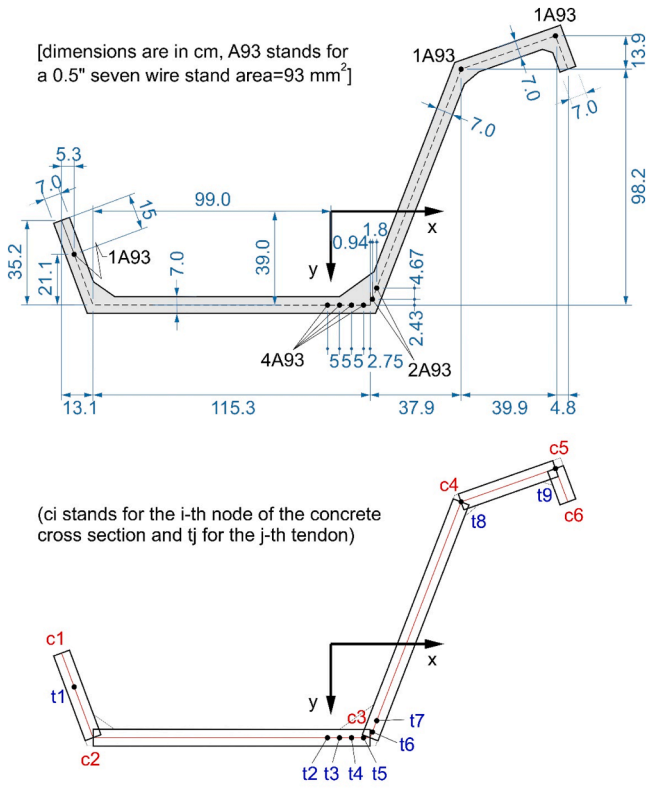

Fig. 10. Geometry of the S shaped beam.

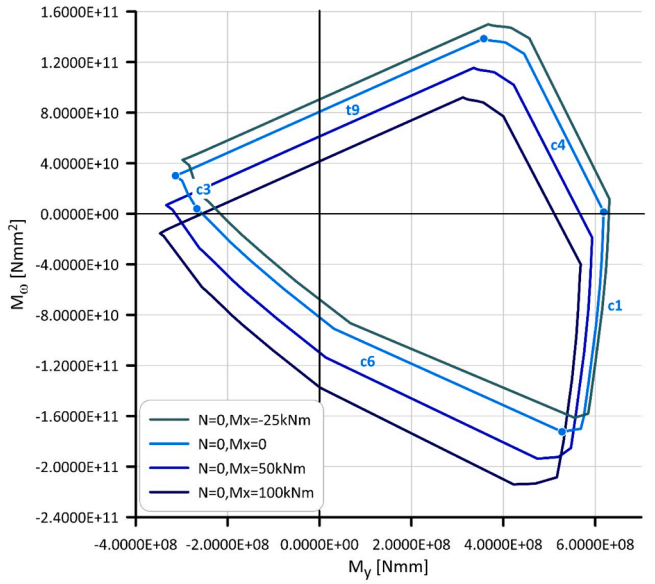

Fig. 11. Interaction diagrams of the S shaped beam of practical interest.

4. Numerical examples

Fig. 4 shows a three-dimensional M_x-M_y-M_ω interaction diagram for $N = 0$. Its projection on the M_y-M_ω plane is shown in Fig. 6. This figure shows that the failure mechanism does not only change in correspondence with the angular points that describe the individual two-dimensional domains, but as M_x varies it also changes on the surface enclosed between such points. In the figure ck stands for the *k*th node of the concrete cross section, rk for the *k*th rebar and tk for the *k*th tendon.

The constitutive laws used are those adopted in the Eurocode 2 [7]. In particular: $f_c = 29.3$ MPa, $f_s = 392.6$ MPa, $\varepsilon_{sy} = 0.001913$, $\varepsilon_{su} = 0.1$, $f_{py} = 1452$ MPa, $\varepsilon_{py} = 0.007225$, $f_{pu} = 1617$ MPa, $\varepsilon_{pu} = 0.06$ and $\bar{\bar{\varepsilon}}_{p_n}(z) = 0.00564 \forall n$.

Similarly, Fig. 8 shows the M_y-M_ω interaction diagrams as the axial action (M_x=0) of the double tee beam depicted in Fig. 7 varies. These diagrams allow the entire domain to be drawn in 3D, which is interesting from a theoretical point of view … but not very useful for engineering practice. Nevertheless, asymmetric, thin-walled, open cross section core walls are particularly common in RC building placed in regions of low-to-moderate seismicity [36], such as Eastern North America [37], Australia [38], and Hong Kong [39]. The approach discussed here applies as is to the analysis of this type of substructures subjected simultaneously to compression, bending and torsion.

The mechanical data adopted are identical to those of the U shaped cross section described previously.

Once again it can be observed that by varying the value of the axial force the failure mechanism can change on a surface of the 3D solid.

The interaction diagrams of the double tee beam of practical interest are shown in Fig. 9.

More complex cross section geometries result in more complicated interaction diagram shapes. An 4example relates to the beam whose geometry is shown in Fig. 10. For it, the interaction diagrams of practical interest are shown in Fig. 11, while Fig. 12 describes some strain distributions, each one corresponding to distinct incipient crisis conditions. The mechanical data adopted are identical to those of the U shaped cross section described previously else than for $f_c = 22.7$ MPa, and for $\bar{\bar{\varepsilon}}_{p_n}(z)$ that now adopts for each tendon the value computed in [13].

Figs. 11 and 12 show interaction diagrams that are not convex. This behaviour is also visible in Fig. 4 if one pays attention to the shape of the lines of the sharp edges of the three-dimensional interaction diagram shown there. This outcome is a consequence of the warping of the cross section.

All the examples described refer to prestressed beams. Since these are ultimate limit state checks and therefore in a cracked regime, it is clear that nothing changes in terms of approach to the problem if the beam is made of reinforced concrete.

5. Conclusions

For over half a century, thin-walled, open cross section PC beams have been widely used in precast structures. However, the problem of determining their load carrying capacity is still unsolved.

A method for plotting interaction diagrams under bending and torsion has been presented.

The advantages of this method are essentially two. First, the systems used consist of two linear equations and only two nonlinear equations, which generally accelerated the speed of convergence compared to systems of the type of Eqs. (6). Furthermore, given its architecture, this method precisely identifies the boundary of the areas in which the section fails due to a given failure mechanism, thus providing a clear and exhaustive description not only of when but also of how the failure occurs for a given combination of internal actions.

The weak point of the method is the ill-conditioning of the system, which, when associated with the non-linearity of two of the four equations involved, makes the problem difficult to solve, especially for combinations far from those for which the structural element was designed.

The interaction diagrams of the thin-walled, open cross section beams are moreover not necessarily convex and therefore differ from those typical of compact cross sections subjected to bending.

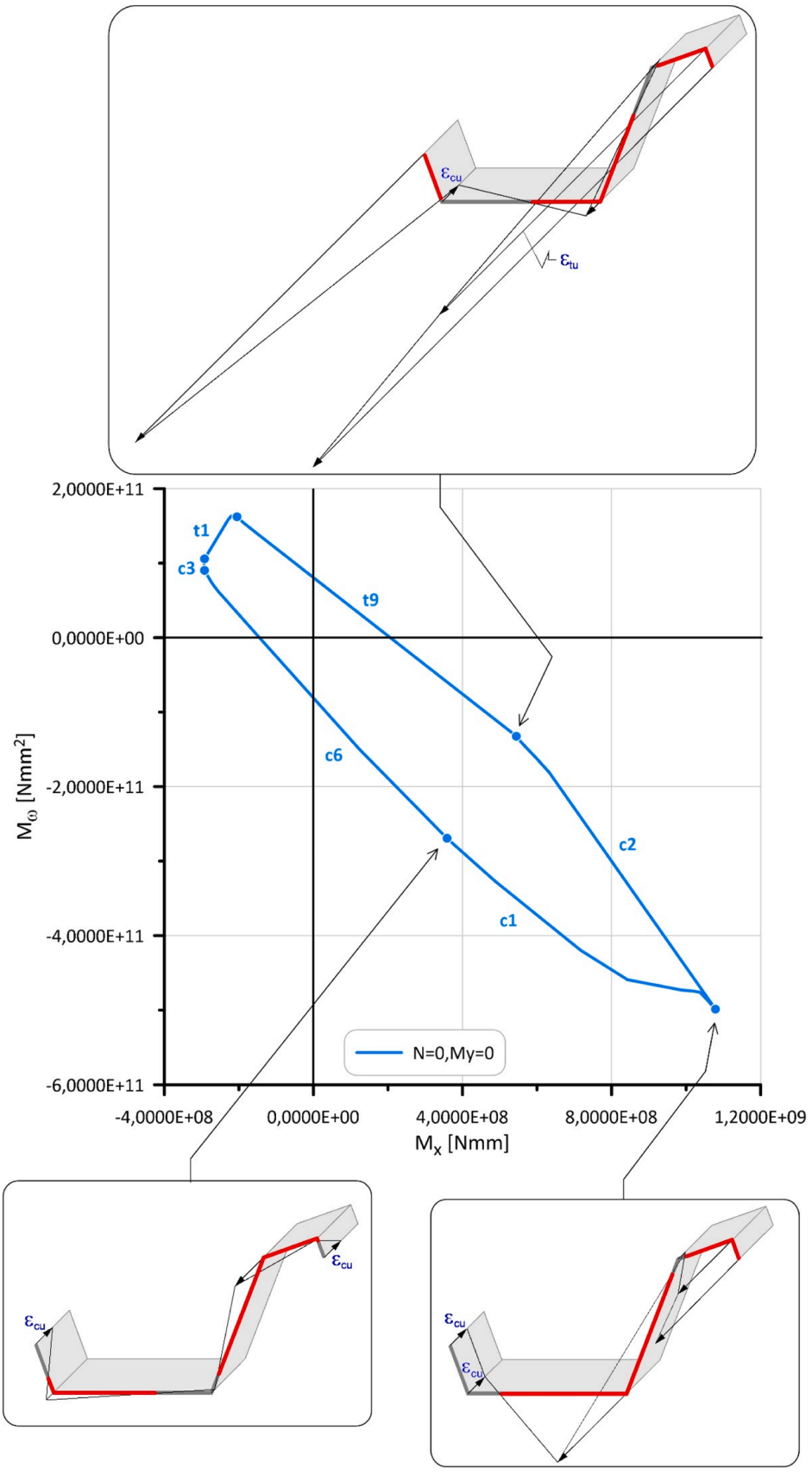

Fig. 12. S shaped beam. Strain distributions corresponding to distinct incipient crisis conditions.

CRediT authorship contribution statement

Marco Andrea Pisani: Writing – original draft, Software, Methodology, Investigation, Formal analysis, Data curation, Conceptualization.

Declaration of competing interest

The authors declare that they have no known competing financial interests or personal relationships that could have appeared to influence the work reported in this paper.

Data availability

Data will be made available on request.

Acknowledgement

This research did not receive any specific grant from funding agencies in the public, commercial, or not-for-profit sectors.

References

[1] V.Z. Vlasov, Novyi metod rascheta prizmaticheskikh balok iz tonkostennykh profilei na sovmestnoe deistvie osevoi sily, izgiba i krucheniya [A new method of designing thin-walled prismatic shells for combined action of axial force, bending and torsion] (in Russian), Vestnik VIA RKKA Im. V.V. Kuibysheva 20(2) (1936).
[2] V.Z. Vlasov, Stroitel'naya Mekhanika Tonkostennykh Prostranstvennykh Sistem [Structural Mechanics of Thin-Walled Spatial Systems], 1949 in RussianMoscow.
[3] V.Z. Vlasov, Thin-walled Elastic Beams, National Science Foundation, Washington DC, 1961.
[4] S.P. Timoshenko, Theory of bending, torsion and buckling of thin-walled members of open cross section, J. Franklin Inst. 239 (1945) 201–219.
[5] S.P. Timoshenko, Theory of bending, torsion and buckling of thin-walled members of open cross section, J. Franklin Inst. 239 (1945) 249–268.
[6] C.F. Kollbrunner, K. Basler, Torsion in Structures, Springer, Berlin, Heidelberg, 1969, https://doi.org/10.1007/978-3-662-22557-8.
[7] European Committee for Standardization, Eurocode 2: Design of Concrete Structures -Part 1-1 : General Rules and Rules for Buildings - EN 1992-1-1, European Committee for Standardization, Bruxelles, Belgium, 2010.
[8] F. Leonhardt, E. Mönnig, Vorlesungen über Massivbau - Teil 1: Grundlagen zur Bemessung im Stahlbetonbau, Springer, Berlin, Heidelberg, 1984, https://doi.org/10.1007/978-3-642-61739-3.
[9] R. El Fatmi, Non-uniform warping including the effects of torsion and shear forces. Part I: a general beam theory, Int. J. Solids Struct. 44 (2007) 5912–5929, https://doi.org/10.1016/j.ijsolstr.2007.02.006.
[10] R. Pavazza, A. Matoković, Bending of thin-walled beams of open section with influence of shear, Part I: theory, Thin-Walled Struct. 116 (2017) 357–368, https://doi.org/10.1016/j.tws.2016.08.027.
[11] R. Pavazza, A. Matoković, M. Vukasović, A theory of torsion of thin-walled beams of arbitrary open sections with influence of shear, Mech. Based Des. Struct. Mach. 50 (2022) 206–241, https://doi.org/10.1080/15397734.2020.1714449.
[12] R. El Fatmi, Non-uniform warping including the effects of torsion and shear forces. Part II: analytical and numerical applications, Int. J. Solids Struct. 44 (2007) 5930–5952, https://doi.org/10.1016/j.ijsolstr.2007.02.005.
[13] M.A. Pisani, Methods for creep analysis of thin-walled precast prestressed concrete beams, J. Eng. Mech. 143 (2017) 04016113, https://doi.org/10.1061/(ASCE)EM.1943-7889.0001191.
[14] M.A. Pisani, Numerical analysis of creep problems, Comput. Struct. 51 (1994) 57–63, https://doi.org/10.1016/0045-7949(94)90036-1.
[15] Z.P. Bažant, S.T. Wu, Dirichlet series creep function for aging concrete, J. Eng. Mech. Div. 99 (1973) 367–387, https://doi.org/10.1061/JMCEA3.0001741.
[16] L. Jendele, D.V. Phillips, Finite element software for creep and shrinkage in concrete, Comput. Struct. 45 (1992) 113–126, https://doi.org/10.1016/0045-7949(92)90349-5.
[17] M. Bocciarelli, M.A. Pisani, Algebrized approach for the finite element analysis of heterogeneous viscoelastic structures, Structures 24 (2020) 783–790, https://doi.org/10.1016/j.istruc.2019.12.016.
[18] B. Belletti, R. Cerioni, I. Iori, Theoretical and experimental analyses of precast prestressed concrete roof elements for large span, in: Proceedings of the 1st International Fib Congress (CD-ROM), JCI-Japan Concrete Institute, Tokyo, 2002.
[19] C. Failla, G. Toniolo, L. Ferrara, Structural design of prestressed precast roof elements made with steel fibre reinforced concrete, in: Proc., 17th Int. BIBM Conf. (CD-ROM), BIBM—European Federation for Precast Concrete, Brussels, Belgium, 2002.
[20] B. Belletti, P. Bernardi, M. Bozzani, G. Todeschini, N. Visconti, A study for the design of thin-webbed prestressed roof elements, in: Proc., 18th Int. BIBM Conf. (CD-ROM), BIBM—European Federation for Precast Concrete, Brussels, Belgium, 2005.
[21] F. Minelli, L. Cominoli, A. Meda, G.A. Plizzari, P. Riva, Full-scale tests on HPSFRC prestressed roof elements subjected to longitudinal flexure, in: Proc., Int. RILEM Workshop on High Performance Fiber Reinforced Cementitious Composites in Structural Applications (CD-ROM), RILEM Publications SARL, Bagneux, France, 2005.
[22] M. Di Prisco, D. Dozio, Thin-webbed open cross-section roof elements: second order effects, in: G.L. Balázs, A. Borosnyói (Eds.), Proc., Fib Symp. on Keep Concrete Attractive, Budapest Univ. of Technology and Economics, Budapest, Hungary, 2005, pp. 619–624.
[23] S. Chen, B. Diao, Q. Guo, S. Cheng, Y. Ye, Experiments and calculation of U-shaped thin-walled RC members under pure torsion, Eng. Struct. 106 (2016) 1–14, https://doi.org/10.1016/j.engstruct.2015.10.019.
[24] B. Belletti, P. Bernardi, E. Michelini, Behavior of thin-walled prestressed concrete roof elements – experimental investigation and numerical modeling, Eng. Struct. 107 (2016) 166–179, https://doi.org/10.1016/j.engstruct.2015.06.058.
[25] J. Xu, S. Chen, Q. Guo, Y. Ye, B. Diao, Y.L. Mo, Experimental and analytical studies of U-shaped thin-walled RC beams under combined actions of torsion, flexure and shear, Int. J. Concrete Struct. Mater. 12 (2018) 33, https://doi.org/10.1186/s40069-018-0245-8.
[26] M. Bottoni, C. Mazzotti, M. Savoia, FEM model for analysis of RC prestressed thin-walled beams, in: 2007.
[27] M. Sekulović, B. Pujević, Nonlinear analysis of reinforced concrete thin-walled beams and frames, Comput. Struct. 32 (1989) 861–870, https://doi.org/10.1016/0045-7949(89)90370-2.
[28] A. Pedron, N. Tondini, Fire behaviour of a prestressed thin-walled concrete V-beam, Fire Technol. 58 (2022) 353–378, https://doi.org/10.1007/s10694-021-01149-3.
[29] K.F. Zbirohowski-Koscia, Stress analysis of cracked reinforced and prestressed concrete thin-walled beams and shells, Mag. Concrete Res. 20 (1968) 213–220, https://doi.org/10.1680/macr.1968.20.65.213.
[30] P. Krpan, M.P. Collins, Testing thin-walled open RC structure in torsion, J. Struct. Div. 107 (1981) 1129–1140, https://doi.org/10.1061/JSDEAG.0005724.
[31] P. Krpan, M.P. Collins, Predicting torsional response of thin-walled open RC members, J. Struct. Div. 107 (1981) 1107–1127, https://doi.org/10.1061/JSDEAG.0005723.
[32] M.A. Pisani, Pre-stressing and Eurocode E.C.2, Eng. Struct. 20 (1998) 706–711, https://doi.org/10.1016/S0141-0296(97)00101-6.
[33] B.P. Demidovic, I.A. Maron, Foundamentals of Numerical Analysis, Mir, Moscow, 1981 in Italian.
[34] J.M. Ortega, W.C. Rheinboldt, Iterative Solution of Nonlinear Equations in Several Variables, Academic Press, 2014.
[35] R.W. Hornbeck, Numerical Methods, Pearson College Div, Englewood Cliffs, N. J, 1982.
[36] R. Hoult, Torsional capacity of reinforced concrete U-shaped walls, Structures 31 (2021) 190–204, https://doi.org/10.1016/j.istruc.2021.01.104.
[37] K. Pelletier, P. Léger, Nonlinear seismic modeling of reinforced concrete cores including torsion, Eng. Struct. 136 (2017) 380–392, https://doi.org/10.1016/j.engstruct.2017.01.042.
[38] R.D. Hoult, E. Lumantarna, H.M. Goldsworthy, Torsional displacement for asymmetric low-rise buildings with RC C-shaped cores, in: Proceedings of the Tenth Pacific Conference on Earthquake Engineering, Bushfire and Natural Hazards CRC, Sydney, Australia, 2015, p. 2015. https://policycommons.net/artifacts/1664175/torsional-displacement-for-asymmetric-low-rise-buildings-with-rc-c-shaped-cores/2395845/ (accessed October 26, 2023).
[39] X.N. Peng, Y.L. Wong, Seismic behavior of asymmetric RC frame building systems with one major wall, in: Proceedings of The 14 Th World Conference on Earthquake Engineering, Beijing, China, 2008.